Journal of Molecular Modeling (2023) 29:140
https://doi.org/10.1007/s00894-023-05547-y

ORIGINAL PAPER

DFT study of adsorbing SO_2, NO_2, and NH_3 gases based on pristine and carbon-doped $Al_{24}N_{24}$ nanocages

R. A. Taha[1] · A. S. Shalabi[1] · M. M. Assem[1] · K. A. Soliman[1]

Received: 19 February 2023 / Accepted: 3 April 2023 / Published online: 14 April 2023

Abstract

The adsorption of SO_2, NO_2, and NH_3toxic gases on $Al_{24}N_{24}$ and $Al_{24}N_{23}C$ nanocages was investigated by using density functional theory (DFT) calculations. The adsorption energies, frontier orbitals, charge transfer using natural bonding orbital (NBO) analysis, dipole moment, the partial density of states (PDOS), thermodynamic relationships, non-covalent interaction (NCI), and quantum theory of atoms in molecules (QTAIM) were considered. The results reveal that carbon-doped $Al_{24}N_{24}$ nanocage increases the adsorption energies for SO_2 and NO_2 gases while decreasing the adsorption energy of NH_3 gas. The ΔG for all configurations were negative except the configurations A1 and G2 confirming the weak adsorption of these two complexes. In conclusion, $Al_{24}N_{24}$ and $Al_{24}N_{23}C$ nanocages are in general promising adsorbents for the removal of SO_2, NO_2, and NH_3 toxic gases. The $Al_{24}N_{24}$ and $Al_{24}N_{23}C$ nanocages are ideal electronic materials.

Keywords $Al_{24}N_{24}$ and $Al_{24}N_{23}C$ nanocage · Toxic gases (SO_2 · NO_2 · And NH_3) · Adsorption · DFT

Introduction

Sulfur dioxide (SO_2), ammonia (NH_3), and nitrogen dioxide (NO_2) are toxic gases that pollute the environment [1, 2]. SO_2 gas is produced by burning petroleum sources and fossil fuels. We can use it in many applications, but it has many problems for human health and causes many diseases such as lung disease, and a high dose of it causes coma or death [3–5]. NH_3 is a colorless gas produced naturally from burning fossil fuels and when used in industry such as plastic production and preparation of nitric acid, it causes many problems such as eye and nose irritation, and a high dose of it may lead to death too [6]. NO_2 is a reddish-brown gas produced by engine combustion producing acid rings, and when it reacts with water, it causes problems to the environment such as damaging buildings and many health hazards [7]. Therefore, the search for new materials to use as sensors that can detect and absorb these gases is aimed. There are several nanostructured materials in zero dimensions (0D), 1D, 2D, and 3D such as nanotubes, nanocages, and nanosheets that have been studied as gas sensors to detect these gases [8–28].

✉ K. A. Soliman
kamal.soliman@fsc.bu.edu.eg; kamalsoliman@gmail.com

[1] Department of Chemistry, Faculty of Science, Benha University, P.O. Box 13518, Benha, Egypt

Derdare et al. used C_{20} and MC_{19} (M = Ru, Ir, and Au) clusters to adsorb and detect NO_2, N_2O, and NH_3 gases by using DFT calculations, and their work showed that adsorption of N_2O and NH_3 on C_{20} is physical adsorption while NO_2 is chemical adsorption, but the change of Eg is very low after adsorption indicating that the sensitivity of C_{20} to these gases is very low. While the doped form of MC_{19}(RuC_{19} and AuC_{19}) sensitivity and stability was increased, the IrC_{19} stability decreased. They also found that it is active and can be used as a catalyst in the decomposition of N_2O gas [29]. Zahedi and Seif [30] show by using DFT calculations that $C_{48}B_6N_6$ heterofullerene is a good material for use as a gas sensor to detect and adsorb NO_2 and NH_3 gases. Rad e al. [31] used pristine graphene (PG) and *N*-doped graphene to adsorb and detect SO_2 and SO_3 gases. They used DFT and NBO calculations and showed that adsorption energy in the case of NDG was higher than in pristine graphene; consequently, NDG is suitable and more detectable for these gases than pristine graphene. Basharnavaz et al. [32] used the P-doped and transition metal (TM)/P-codoped graphitic carbon nitride (gCN) systems (TM = Co, Rh, and Ir elements) to adsorb and detect SO_2 gas. This work by using DFT calculations showed that TM/P-codoped gCN systems have adsorption energy higher than that of the pristine gCN. Also, they found that the Ir/P-codoped gCN was a better system for adsorption and detection of the SO_2 gas compared with

other systems with a high adsorption energy of − 3.52 eV. Zhang et al. [27] used graphene for the adsorption of SO_2 by using DFT calculations. They showed that there were four structures for graphene, namely, pristine graphene (PG), vacancy-defected graphene (VG), Ti-doped graphene (Ti-G), and Ti-doped graphene with vacancies (Ti-VG). Their results showed that Ti-doped graphene is the best structure for the adsorption of SO_2 gas with the highest adsorption energy. Noei [33] explained the electronic properties of pristine $Al_{12}N_{12}$ and $B_{12}N_{12}$ nanoclusters for the adsorption of SO_2 gas. The results show that the two structures are sensitive to adsorb SO_2 gas. Rad and Ayub [34] study the adsorption of O_3 and SO_2 molecules on pristine $B_{12}N_{12}$ and Ni-decorated $B_{12}N_{12}$ nanocages. They showed that the Ni-decorated $B_{12}N_{12}$ enhances and increases the adsorption of these gases. Xi et al. [35] examined the adsorption of CO_2 molecules on two stable BiC and Bi2C monolayers promising adsorbents to capture CO_2 gas. Zhao et al. [36] proposed a single metal catalyst on a 2D BC3N2 substrate for the activation of CO_2 and CH_4 gasses into CH_3COOH. Huo et al. [37] used $Fe_{36}Co_{44}$ nanostructure to catalyze the hydrolysis reaction of ammonia borane to produce H_2. Zhang et al. [38] study the removal of COS chemicals by nano-hollow sphere hydrolytic catalyst. Zhao e al. [39] investigated the 2D-InSe with B-doped as bifunctional catalysts to separate CO_2 and CH_4 under the regulation of an external electric field.

In this work, we study the adsorption of three toxic gases on $Al_{24}N_{24}$ and $Al_{24}N_{23}C$ nanocages by using DFT calculations to decrease air pollution. The adsorption energies, NBO, PDOS, NCI, and QTAIM were determined.

Computational details

In this study, all the geometries of nanocages and gas molecules before and after adsorption on nanocages were fully optimized based on density functional theory (DFT) without any symmetry constraint. The B3LYP and 6-31 g(d) level of theory were used for NO_2 and SO_2 systems and 6-31 g(d,p) for NH3 systems. The calculations were carried out by Gaussian 09 [40]. The adsorption energy of a gas molecule on the nanocages was obtained from the following equation:

$$E_{ads} = E_{gas@nanocage} - E_{gas} - E_{nanocage} \quad (1)$$

where $E_{gas@nanocage}$, E_{gas}, and $E_{nanocage}$ are the total energy of the gas molecule on the nanocage ($Al_{24}N_{24}$ and $Al_{24}N_{23}C$), the total energy of the gas molecule, and the total energy of the nanocage ($Al_{24}N_{24}$ and $Al_{24}N_{23}C$), respectively.

Thermodynamic parameters at $T = 298.15$ K and $P = 1$ atm such as Gibbs-free energy change (ΔG), enthalpy change (ΔH), and entropy change (ΔS) of the adsorption were evaluated.

Results and discussion

Geometry analysis

The adsorption capacity, which is one of the most important parameters that determine catalytic activity, indicates the selectivity of a particular substance by comparing it with other materials [41–43]. In this work, theoretical methods were used to study the adsorption of three industrial gases NO_2, SO_2, and NH_3 based on the adsorbent material $Al_{24}N_{24}$ nanocage. As evident from Fig. 1, the nanocage of $Al_{24}N_{24}$ consists of 12 tetragons, 8 hexagons, and 6 octagons. As seen in Fig. 1, in pristine $Al_{24}N_{24}$, the bond distances between nitrogen and aluminum that are shared between 6- and 8-membered rings are 1.78 Å, 4- and 8-membered rings are 1.83 Å, and for 4- and 6-membered rings are 1.86 Å. By the replacement of one nitrogen with one carbon atom ($Al_{24}N_{23}C$ nanocage), the bond distance between the doping atom and aluminum atom increases by 0.11 and 0.12 Å in comparison with pristine $Al_{24}N_{24}$.

Electrostatic potential map (ESP) is a useful tool for predicting the reactivity sites for a nucleophilic and electrophilic attack. As shown in Fig. 1, the red and blue colors represent the regions of negative (related to electrophilic reactivity) and positive (related to nucleophilic reactivity) electrostatic potential respectively. The negative regions are localized on the N atom, and the positive regions of ESP are localized on Al and C atoms.

Interaction of NO_2, SO_2, and NH_3 with $Al_{24}N_{24}$ and $Al_{24}N_{23}C$ nanocages

The optimized geometry configurations of NO_2 on $Al_{24}N_{24}$ and $Al_{24}N_{23}C$ nanocages are shown in Fig. 2. The three different configurations of NO_2 on $Al_{24}N_{24}$ are represented as A1 to C1 and A2 to C2 for $Al_{24}N_{23}C$ nanocages. Configuration A1 displays a nitrogen atom in a NO_2 molecule interacting with an aluminum atom of pristine $AL_{24}N_{24}$ nanocage presented in Table 1, by distance 2.12 Å and adsorption energy − 0.19 eV. In complex A2, the NO_2 molecule interacting with the doped carbon $Al_{24}N_{24}$ nanocage is different from that in configuration A1; the NO_2 molecule interacts through nitrogen with carbon-doped $Al_{24}N_{24}$ and oxygen with the aluminum atom of $Al_{24}N_{23}C$. The additional interaction C of figuration A2 is responsible for strong binding energy by forming a C–N bond with a distance of 1.39 Å and the adsorption energy − 3.65 eV. A comparison between complex A1 and B1 indicates that the oxygen atom in the NO_2 molecule strongly interacts with pristine $Al_{24}N_{24}$ nanocage as in complex B1, while in complex B2, by carbon-doped Al24N24, the interaction of nitrogen and oxygen atoms in NO_2 is stronger than the two oxygen atoms of NO_2 molecule. As seen in Table 1, the results reveal that adsorption energies

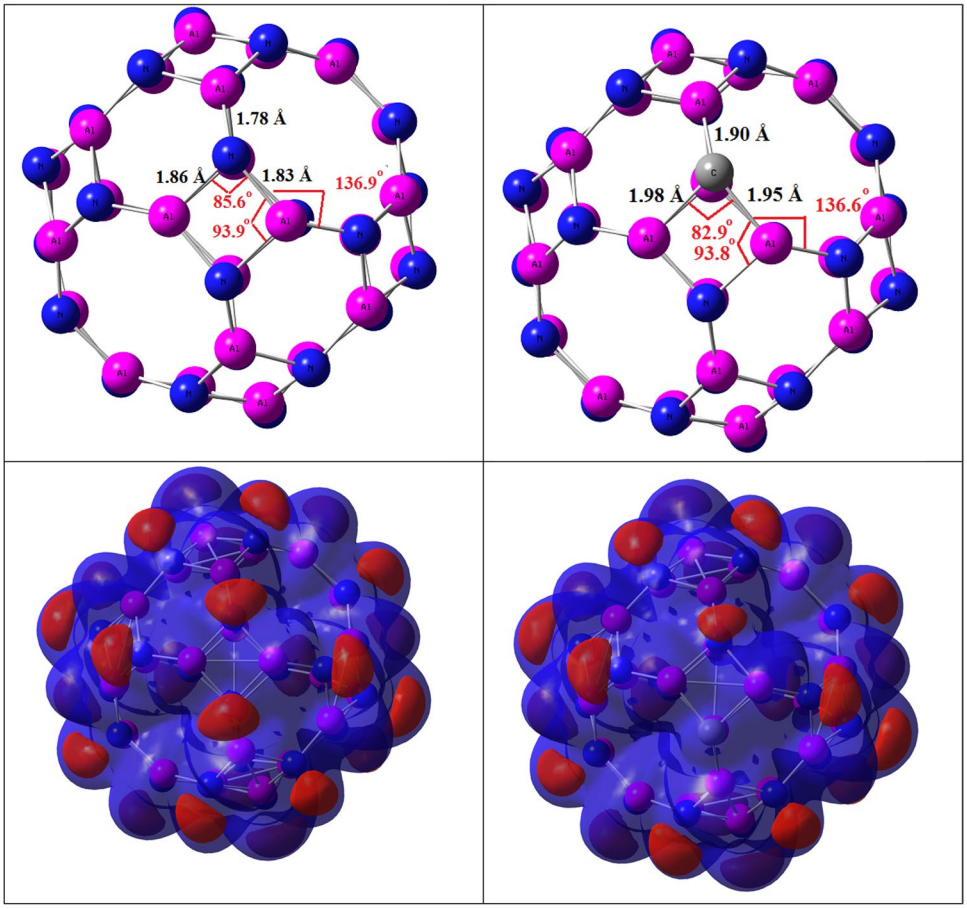

Fig. 1 The optimized geometries and electrostatic potential map (ESP) of $Al_{24}N_{24}$ and $Al_{24}N_{23}C$

are enhanced by carbon doping $Al_{24}N_{24}$. As shown in complex C1 and C2 in Fig. 2, the interaction of nitrogen in NO_2 molecule is attracted by nitrogen of pristine $Al_{24}N_{24}$ and carbon of $Al_{24}N_{23}C$ leading to the formation of N–N bond in pristine $Al_{24}N_{24}$ and C–N bond in $Al_{24}N_{23}C$ nanocage. The bond lengths in both complex C1(N–N) and C2 (C-N) are 1.40 Å and 1.30 Å respectively.

For SO_2 gas adsorbed on the two nanocages $Al_{24}N_{24}$ and $Al_{24}N_{23}C$, the most stable orientations D1 and E1 for $Al_{24}N_{24}$, D2, and E2 for $Al_{24}N_{23}C$ nanocages are depicted in Fig. 3. The adsorption energies for SO_2 molecules in orientations D1 and D2 as shown in Table 2 are – 0.58 eV and – 2.10 eV, respectively. The interactions of the complex D1 and D2 are different like complex B1 and B2 of NO_2 adsorbed on $Al_{24}N_{24}$ and $Al_{24}N_{23}C$. The presence of carbon doped in $Al_{24}N_{24}$ leads to improving the adsorption energy by about 3.62 times $Al_{24}N_{24}$ nanocage. The interaction of the sulfur atom in the SO_2 molecule with the nitrogen of $Al_{24}N_{24}$ and carbon-doped $Al_{24}N_{23}C$ is stronger as in orientations E1 and E2. The adsorption energies of the complexes E1 and E2 are – 2.58 eV and – 3.10 eV respectively.

The response of carbon-doped $Al_{24}N_{24}$ nanocage is decreased towards the NH_3 gas molecule. As shown in Fig. 4, there are three configurations for the adsorption of NH_3 gas on $Al_{24}N_{24}$ and carbon-doped $Al_{24}N_{23}C$, the configuration F1, and the NH_3 molecule prefers to lie on the aluminum atom of $Al_{24}N_{24}$ with adsorption energy – 1.41 eV as in Table 3. In configurations F2 and G2, NH_3 binds with aluminum and carbon of $Al_{24}N_{23}C$, and the calculated adsorption energies for the complex F2 and G2 are – 1.36 eV and 0.41 eV showing that the interaction of NH_3 with the carbon of $Al_{24}N_{23}C$ is physical adsorption.

When the gas is adsorbed physically, we can reuse the substrate, while if a chemical bond is formed between the gas molecule and the substrate; it means that the desorption process is difficult. As presented in Tables 1 and 2, the doped $Al_{24}N_{24}$ by carbon atom for SO_2 and NO_2 molecules is chemically adsorbed, so this nanocage is not suitable for sensing SO_2 and NO_2 gas molecules. In the case of NH_3 systems, the binding of the NH_3 gas molecule with the aluminum atom as seen in Table 3 configuration F2 is lower in adsorption energy than configuration F1. As revealed from their results, pristine $AL_{24}N_{24}$ nanocage is sensitive to the three gas molecules while carbon-doped ($Al_{24}N_{23}C$) nanocage is sensitive only to NH_3 gas molecule. We propose a diagnostic test for the effect of the basis set by

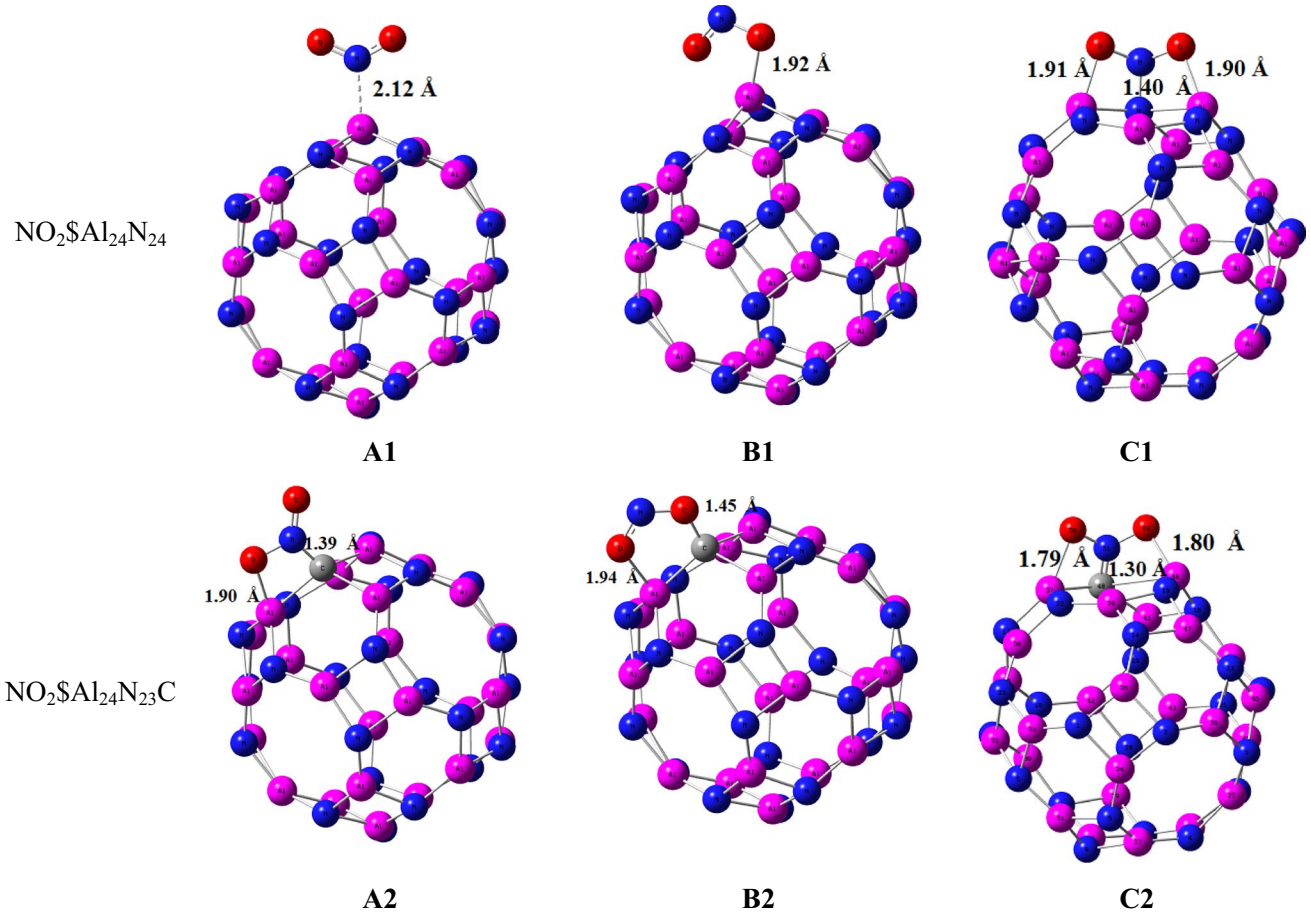

Fig. 2 Adsorption configurations of NO_2 on $Al_{24}N_{24}$ and $Al_{24}N_{23}C$

Table 1 Structural parameters of NO_2 adsorbed on $AL_{24}N_{24}$ and $AL_{24}N_{23}C$ nanocage. The value between brackets is calculated by the cc-PVDZ basis set

	d (Å)	Eads (eV)	HOMO (eV)	LUMO (eV)	ΔE (eV)	μ (Debye)	Q_{NBO}
$Al_{24}N_{24}$	–	–	−6.48	−2.39	4.09	0.0068	–
$Al_{24}N_{23}C$	–	–	−6.35	−2.34	4.01	0.6913	–
NO_2\$$Al_{24}N_{24}$ (A1)	2.12	−0.19 (−0.19)	−6.40	−2.48	3.92	4.2998	−0.302
NO_2\$$Al_{24}N_{23}C$ (A2)	1.39, 1.90	−3.65 (−3.51)	−6.40	−2.48	3.92	4.0570	−0.467
NO_2\$$Al_{24}N_{24}$ (B1)	1.92	−0.95 (−0.91)	−6.46	−2.48	3.98	4.4967	−0.61
NO_2\$$Al_{24}N_{23}C$ (B2)	1.45, 1.94	−3.14 (−3.03)	−6.31	−2.75	3.56	2.7965	−0.374
NO_2\$$Al_{24}N_{24}$ (C1)	1.90, 1.40, 1.91	−1.41 (−1.33)	−6.42	−2.43	3.99	3.9002	0.47
NO_2\$$Al_{24}N_{23}C$ (C2)	1.80, 1.30, 1.79	−3.83 (−3.66)	−6.31	−2.47	3.84	3.7162	−1.007

using cc-PVDZ as a single-energy calculation, as seen in Tables 1, 2, and 3; the calculated adsorption energies show change ranges from 0 to 0.17 eV in the case of NO_2, from 0.11 to 0.31 eV for SO_2, and from 0.01 to 0.05 eV for NH_3 as we compare with the basis set used for this study mentioned in computational details.

NBO charges and dipole moment

The dipole moment and the charge transfer for the adsorbed gases on pristine $Al_{24}N_{24}$ and carbon-doped $Al_{24}N_{23}C$ nanocages were investigated. As seen in Table 1, the dipole moment of the pristine $Al_{24}N_{24}$ nanocage is 0.0068 Debye. After doping with carbon, the dipole moment was changed

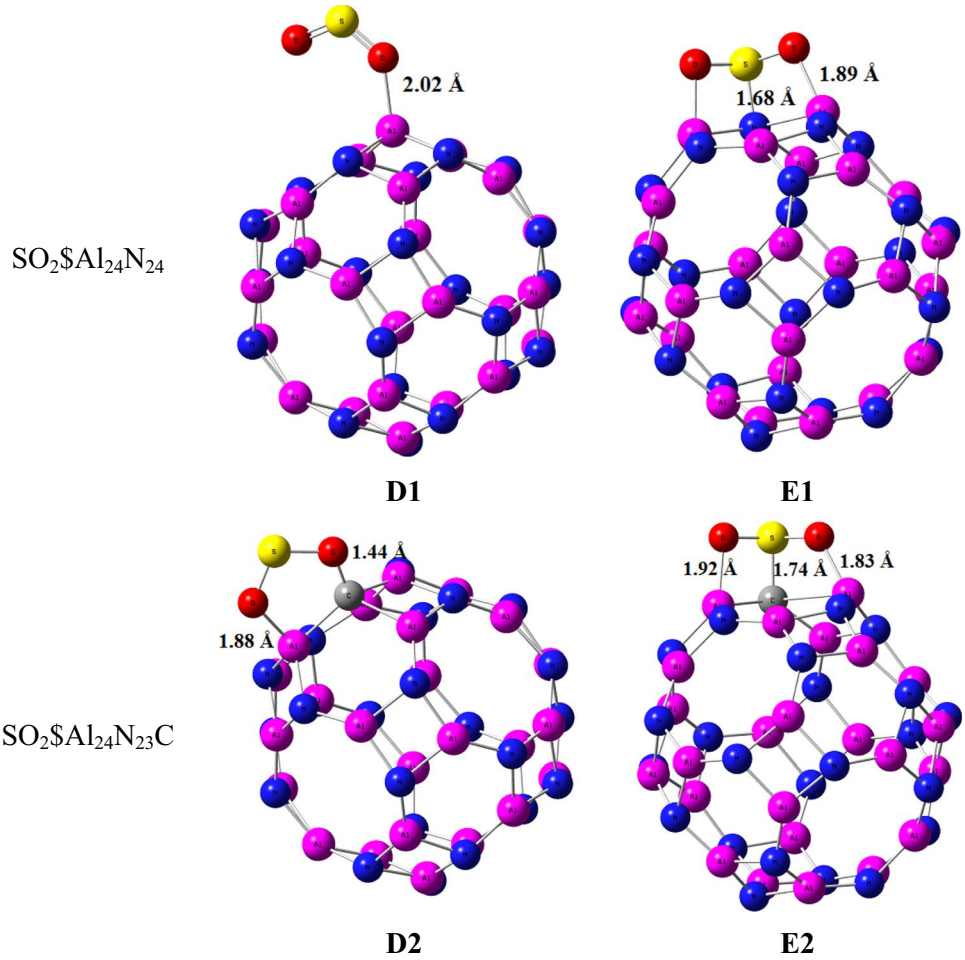

Fig. 3 Adsorption configurations of SO_2 on $Al_{24}N_{24}$ and $Al_{24}N_{23}C$

Table 2 Structural parameters of SO_2 adsorbed on $AL_{24}N_{24}$ and $AL_{24}N_{23}C$ nanocage. The value between brackets is calculated by the cc-PVDZ basis set

	d (Å)	Eads (eV)	HOMO (eV)	LUMO (eV)	ΔE (eV)	μ (Debye)	Q_{NBO}
SO_2\$$Al_{24}N_{24}$ (D1)	2.02	−0.58 (−0.73)	−6.20	−4.97	1.23	5.1966	0.06
SO_2\$$Al_{24}N_{23}C$ (D2)	1.44, 1.88	−2.10 (−2.41)	−5.73	−2.33	3.40	3.0320	−0.501
SO_2\$$Al_{24}N_{24}$ (E1)	1.68, 1.89	−2.58 (−2.79)	−6.34	−2.40	3.94	3.3922	−0.3
SO_2\$$Al_{24}N_{23}C$ (E2)	1.92, 1.74, 1.83	−3.10 (−3.31)	−6.28	−2.36	3.92	3.5360	−0.494

to 0.6913 Debye. The adsorption of NO_2, SO_2, and NH_3 gases on the two nanocages brings a change in the dipole moment. As seen in Fig. 5, the dipole moment vectors of the SO_2 and NO_2 adsorbed on $Al_{24}N_{24}$ and $Al_{24}N_{23}C$ nanocages point away from these two groups. For configuration D1 where the SO_2 group is adsorbed on $Al_{24}N_{24}$ nanocage, the dipole moment vector points forward to this group. For the NH_3 group adsorbed on $Al_{24}N_{24}$ and $Al_{24}N_{23}C$ nanocages, the directions of dipole moment vectors point forward to this group. The charge transferred was determined for all complexes. As seen in Tables 1, 2, and 3, the charge transfers from the nanocage to the SO_2 and NO_2 gas molecules due to the withdrawing nature of the SO_2 and NO_2 molecules. For configuration C1, this is due to N–N bond formation between NO_2 gas and $Al_{24}N_{24}$ nanocage and for configuration D1 because SO_2 binds to the $Al_{24}N_{24}$ through an oxygen atom of SO_2 molecule. As a comparison between configuration A2 and C2 where NO_2 adsorbs on carbon-doped nanocage ($Al_{24}N_{23}C$), the value of charge transferred for configuration C2 is larger than in configuration A2; this indicates stronger interaction between NO_2 and nanocage in configuration C2 than that of configuration A2. Note that when the value of charge transfer increases, a strong interaction between gas molecules and substrates occurs. For NH_3 systems, the charge is transferred from the gas molecule to the nanocage.

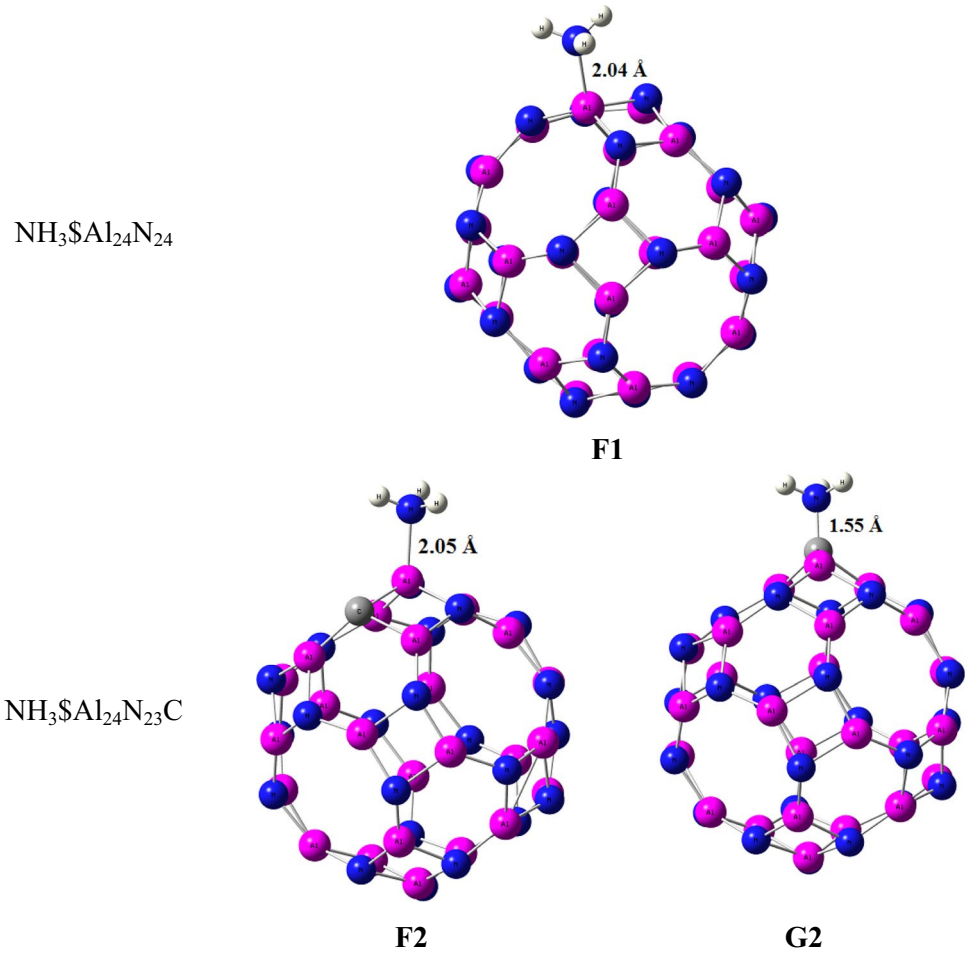

Fig. 4 Adsorption configurations of NH_3 on $Al_{24}N_{24}$ and $Al_{24}N_{23}C$

Table 3 Structural parameters of NH_3 adsorbed on $AL_{24}N_{24}$ and $AL_{24}N_{23}C$ nanocage. The value between brackets is calculated by the cc-PVDZ basis set

	d (Å)	Eads (eV)	HOMO (eV)	LUMO (eV)	ΔE (eV)	μ (Debye)	Q_{NBO}
NH_3\$$Al_{24}N_{24}$ (F1)	2.04	− 1.41 (− 1.4)	− 6.11	− 2.13	3.97	6.7408	0.13
NH_3\$$Al_{24}N_{23}C$ (F2)	2.05	− 1.36 (− 1.35)	− 5.90	− 2.08	3.82	7.4192	0.137
NH_3\$$Al_{24}N_{23}C$ (G2)	1.55	0.41 (0.36)	− 6.11	− 2.24	3.87	6.7271	0.485

Thermodynamic parameters and density of states

The analysis of interaction energies is expanded to include enthalpies (H), Gibbs-free energies (G), and entropies (S) of interaction. The thermodynamic parameters for the adsorbed gases SO_2, NO_2, and NH_3 such as Gibbs-free energy change (ΔG), enthalpy change (ΔH), and entropy change (ΔS) were determined at $T = 298.15$ K and $P = 1$ atm.

As seen in Table 4, the negative values of Gibbs-free energies indicate the spontaneous adsorption of gases molecule on the two nanocages. The higher value of ΔG implies a strong interaction between the gas molecule and substrate. The enthalpy change values are higher than the Gibbs-free energy values which indicate that the enthalpy is stabilized. The ΔG for the configurations A1 and G2 have a positive value confirming weak adsorption for these complexes.

In Tables 1, 2, and 3, the quantum parameters and the electronic properties of the gaseous molecule were evaluated. The HOMO of most complexes is shifted to higher energy. The HOMOs of adsorbed gases were comparable. After the adsorption of this NO_2, SO_2, and NH_3 on the $Al_{24}N_{24}$ and $Al_{24}N_{23}C$, the energy gap for all systems decreased.

The PDOS analysis

To characterize the interactions between SO_2, NO_2, and NH_3 gases with the study nanocages ($Al_{24}N_{24}$ and $Al_{24}N_{23}C$), the projected density of states (PDOS) was examined.

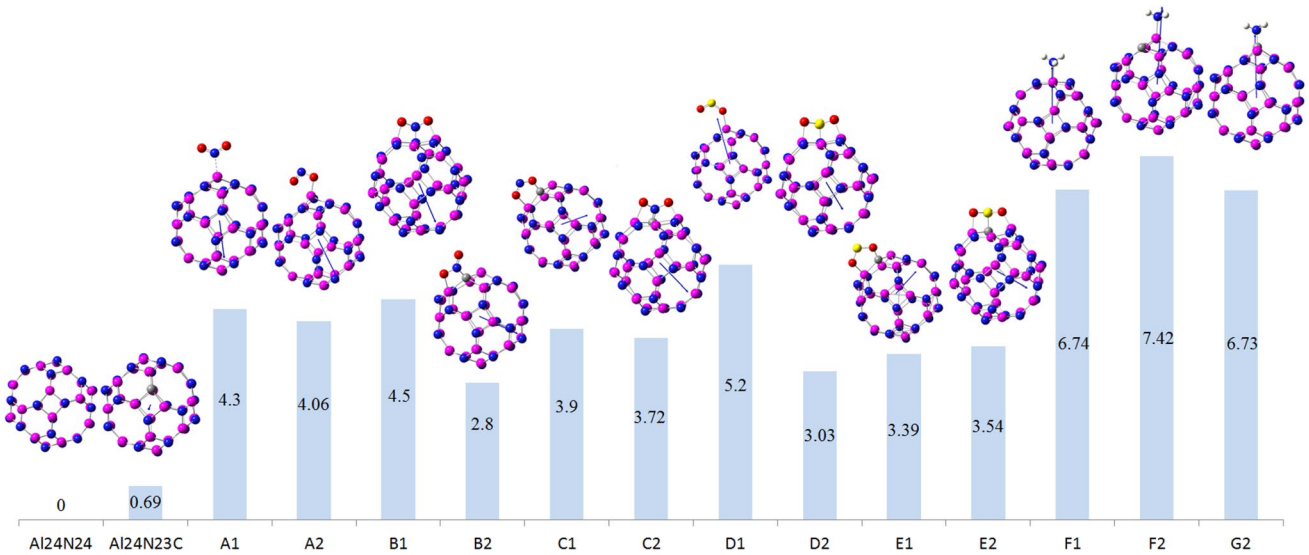

Fig. 5 Dipole moment directions for the two nanocages together with the adsorbed gas molecules

Table 4 Thermodynamic parameters of the gas molecules adsorbed on nanocages

	ΔG (Kcal/mole)	ΔH (Kcal/mole)	ΔS (Cal/mole-K)
NO2$Al24N24 (A1)	5.81	− 3.52	− 31.295
NO2$Al24N23C (A2)	− 68.02	− 81.77	− 46.098
NO2$Al24N24 (B1)	− 10.67	− 21.40	− 35.98
NO2$Al24N23C (B2)	− 56.63	− 70.66	− 47.04
NO2$Al24N24 (C1)	− 17.85	− 31.39	− 45.41
NO2$Al24N23C (C2)	− 71.87	− 86.33	− 48.485
SO2$Al24N24 (D1)	− 2.45	− 12.34	− 33.19
SO2$Al24N23C (D2)	− 34.82	− 47.42	− 42.252
SO2$Al24N24 (E1)	− 44.34	− 58.25	− 46.67
SO2$Al24N23C (E2)	− 56.67	− 70.24	− 45.51
NH3$Al24N24 (F1)	− 20.55	− 30.36	− 32.89
NH3$Al24N23C (F2)	− 19.63	− 29.17	− 31.99
NH3$Al24N23C (G2)	21.91	11.52	− 34.86

After adsorbing SO_2, NO_2, and NH_3 gases on $Al_{24}N_{24}$ and $Al_{24}N_{23}C$, the PDOS of O-2sp, N-2sp, C-2sp, S-3sp, NH_3-sp, Al-3 s, and Al-3p orbitals was displayed in Figs. 6, 7, 8, and 9. It is important to note that the charge transfers from Al to the anti-bonding states of NO_2 and SO_2 molecule that elongates the N–O and S–O bond to 1.341 Å, and 1.372 Å at C2 and E2, respectively. It was shown that the O-2sp, N-2sp, and S-3sp orbitals were found to be particularly localized close to the Fermi level; facilitating their interactions with the C-2sp, Al-3 s, and Al-3p states in $Al_{24}N_{23}C$ nanocage indicates the NO_2 and SO_2 may have a higher binding energy (E_b) if it is close to the C atom in the $Al_{24}N_{23}C$ nanocage. Figure 6 shows that the Al-3 s and Al-3p orbitals are pushed to lower energies as a result of electron transfer from the Al atoms to the NO_2 and SO_2 molecules, which considerably aids in the adsorption of NO_2 and SO_2.

By the binding energies indicated in Tables 1 and 2, it is seen that the Al-3p orbitals of C2′s PDOS display increased intensity, indicating that C2 is more significant than both E2 and C1 configurations. Furthermore, from − 6.20 to − 12.70 eV, the N-2sp states of adsorbed NO_2 contribute significantly to the C-2sp (HOMO), indicating that the C atom uses its valence orbitals to interact with the O-2sp, N-2sp, Al-3 s, and Al-3p states of NO_2 as well as the $Al_{24}N_{23}C$ nanocage. Due to the distribution of S-3sp states in a broad range from − 5.40 to − 14.30 eV (E2) below the Fermi level, the S-3sp orbitals of SO_2 also show a stronger hybridization with the C-2sp, Al-3 s, and Al-3p orbitals of $Al_{24}N_{23}C$. Agreeing with their binding energies, the charge-transfer values between the S, N, and C atoms of NO_2 and SO_2 and the $Al_{24}N_{23}C$ nanocage suggest that

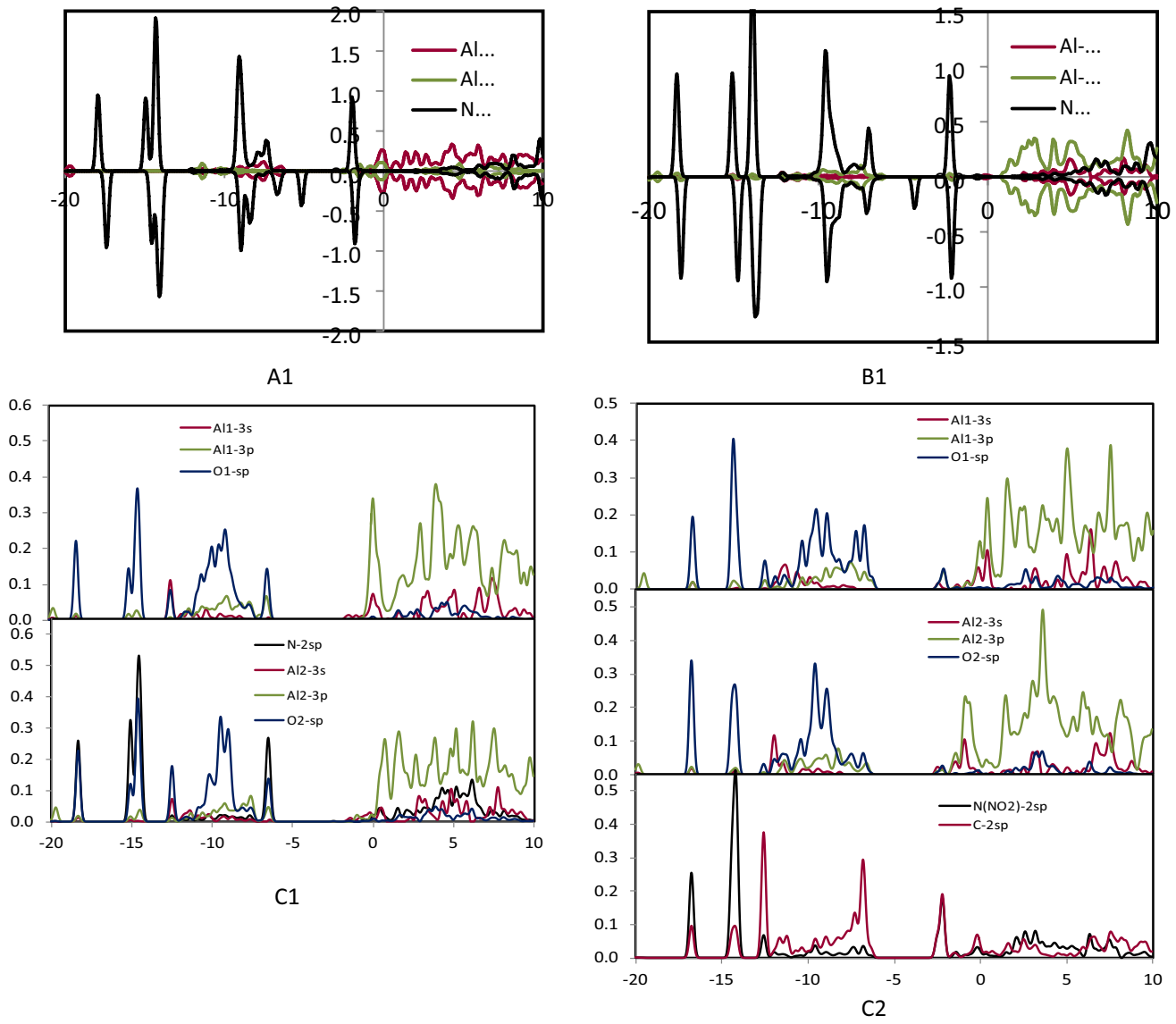

Fig. 6 PDOS of configuration A1, B1, C1, and C2

Fig. 7 PDOS of configuration D1 and D2

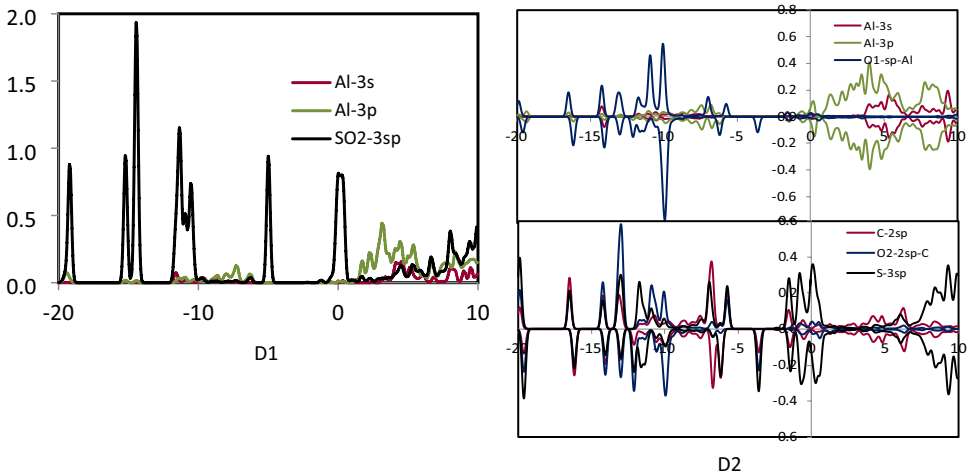

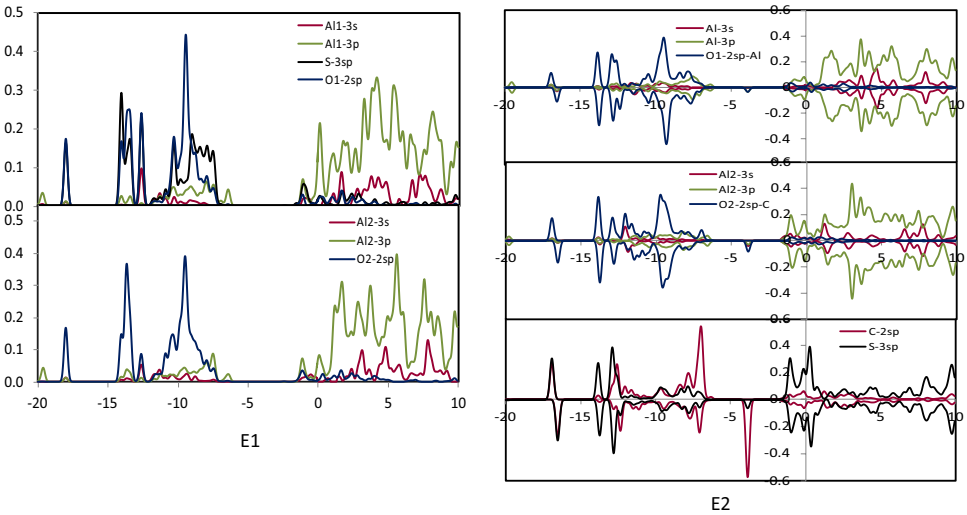

Fig. 8 PDOS of configuration E1 and E2

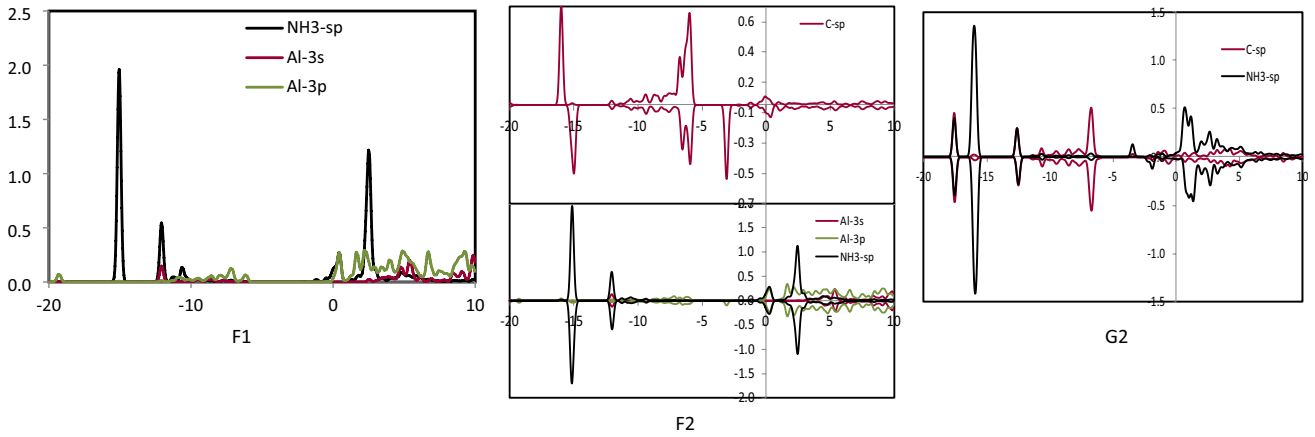

Fig. 9 PDOS of configuration F1, F2, and G2

the charge-transfer is more important for the stability of these complexes than the electrostatic interactions. On the other hand, a weak connection between the substrate and the NH_3 molecule results from the soft hybridization of the NH_3 and $Al_{24}N_{23}C$'s C-2p orbitals.

Non-covalent interaction (NCI) analysis

To identify non-covalent bonds, such as hydrogen bonds, steric clashes, Van der Waals (vdW), and reduced density gradients, the quantum mechanical electron density has been used (RDG) determined by the following equation:

$$RDG(r) = \frac{1}{2(3\pi^2)^{1/3}} \frac{|\nabla\rho(r)|}{\rho(r)^{4/3}} \quad (2)$$

where the ρ value can represent the bond strength, whereas the value of $\text{sign}(_2) \times \rho$ is used to evaluate the nature of the interaction between the SO_2, NO_2, and NH_3 gases and the investigated nanocages ($Al_{24}N_{24}$ and $Al_{24}N_{23}C$). $_2$ is the second-largest eigenvalue of the electron density in the Hessian matrix, where $\text{sign}(_2) \times \rho < 0$ denotes an attractive interaction and $\text{sign}(_2) \times \rho > 0$ denotes a repulsive interaction.

To study the non-covalent interactions between the NO_2, SO_2, and NH_3 gases and the investigated nanocages, the scatter graphs between the reduced density gradient (RDG) and the electron density (ρ) have been shown in Figs. 10 and 11. As seen in Figs. 10 and 11, $\text{sign}(\lambda_2)\rho)$ increases for red areas suggesting high steric repulsions inside the nanocage, whereas $\text{sign}(\lambda_2)\rho$ decreases for blue areas indicating strong contacts. The green areas between the complex's elements approaching 0 are Van der Waals interactions, which are weak intermolecular forces. The considerable vdW

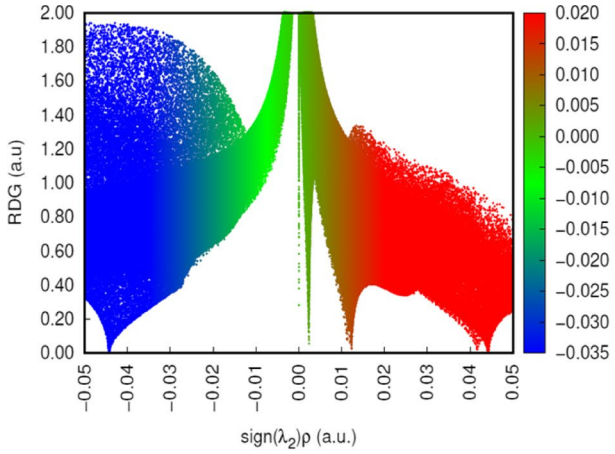

$Al_{24}N_{23}C$ nanocage

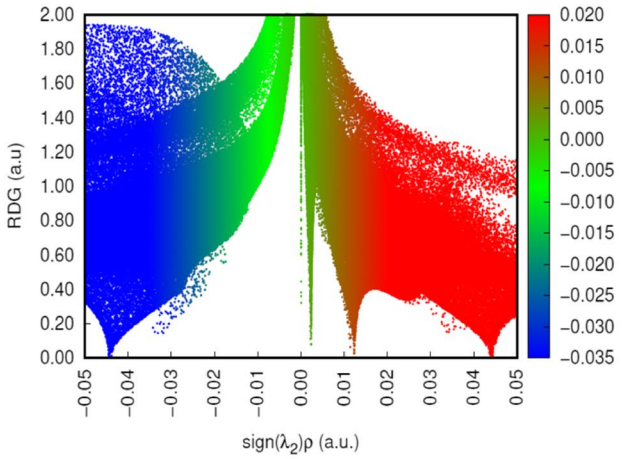

A1

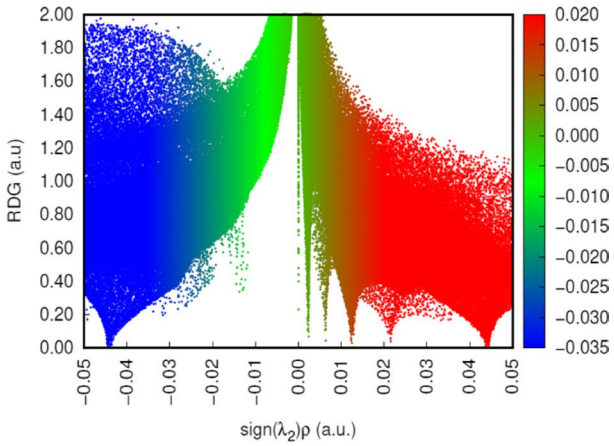

C2

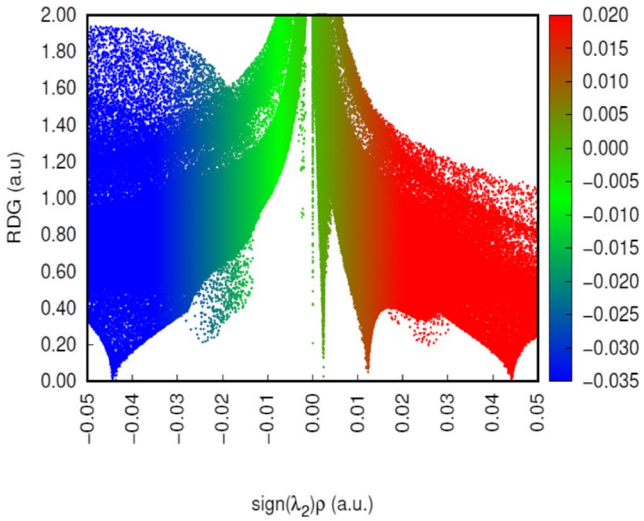

D1

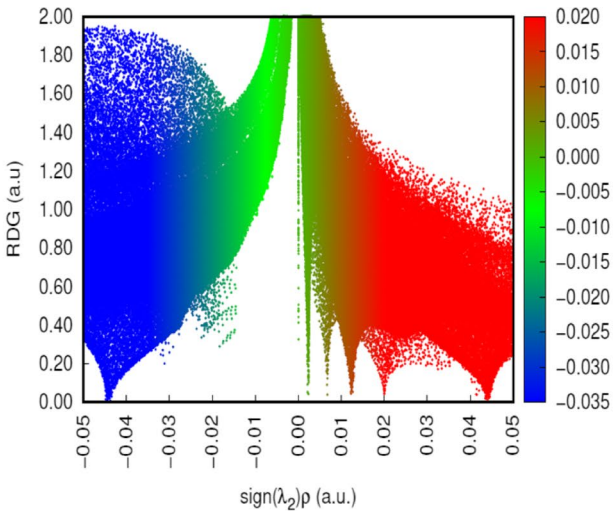

E2

Fig. 10 Non-covalent interaction of G2 and F1

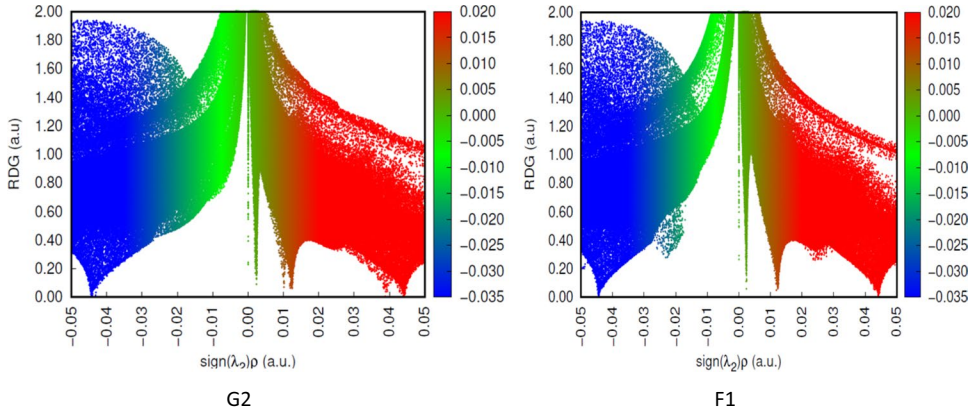

Fig. 11 Non-covalent interaction of $Al_{24}N_{23}C$ nanocage, A1, C2, D1, and E2

interaction between the NH_3 and the $Al_{24}N_{23}C$ (G2) nanocages is visible, as can be seen in Fig. 11. This conclusion is supported by the geometric analysis, which considers weak interactions.

Additionally, blue and green blended spikes were seen at greater electron densities and $\text{sign}(\lambda_2)\rho < 0$, which shows that the C2, E2, and F1 complexes have developed partial covalent connections. The blue and green patches between the gas molecule and the nanocages, as well as the intermolecular contact, were visible in the partial covalent bond as shown in Figs. 10 and 11. Higher interaction intensity was seen for C2 and E2 configurations due to the partial covalent contact between the SO_2 and NO_2 molecules with the $Al_{24}N_{23}C$ nanocage in the RDG versus $\text{sign}(_2) \times \rho$ graph.

Quantum theory of atoms in molecules (QTAIM)

A well-known method for examining the topology of interactions is QTAIM (covalent or non-covalent). For the most stable configuration of C2, E2, and F1 complexes, measurements of several topological parameters, including electron density (ρ_r), Laplacian ($\nabla^2 \rho_r$), and total electron energy density (H_r) at the bond critical points (BCP), have been made in order to characterize the strength and type of bond (Table 5). Shared shell interactions (covalent bonds) exist when the ρ_r is larger than 0.20 a.u., is higher than 0.20 a.u, and the Laplacian is higher but negative. Al24N23C nanocage's Al-to-carbon bond is demonstrated to be partially covalent in the presence of $\nabla^2 \rho_r > 0$ and $Hr < 0$ [44]. However, $\rho_r < 0.1$ a.u [45] indicates closed-shell interactions (ionic, hydrogen bonding, or van

Table 5 The topological parameters, including electron density (ρ_r), Laplacian of electron density ($\nabla^2\rho_r$), the density of kinetic energy (G_r), the density of potential energy (V_r), and the density of total energy (H_r) in (a.u.) at the bond critical point (BCPs) for the most stable configurations C2, E2, and F1

Structure	Bonds	ρr	$\nabla^2 \rho r$	Gr	Vr	Hr
C2	N–O	0.346	−0.446	0.224	−0.559	−0.336
	N–O	0.378	−0.540	0.254	−0.644	−0.389
	N–C	0.326	0.373	0.607	−1.121	−0.514
	Al1–O	0.072	0.502	0.122	−0.118	0.004
	Al2–O	0.055	0.304	0.077	−0.079	−0.001
	Al–C	0.068	0.277	0.084	−0.099	−0.015
E2						
	Al–C	0.065	0.264	0.078	−0.091	−0.012
	Al1–O	0.061	0.389	0.095	−0.093	0.002
	Al2–O	0.072	0.528	0.126	−0.119	0.006
	S–O	0.227	0.112	0.293	−0.558	−0.265
	S–O	0.207	−0.043	0.221	−0.453	−0.232
	S–C	0.216	−0.398	0.070	−0.240	−0.170
F1						
	Al–N	0.050	0.272	0.067	−0.066	0.001
	N–H	0.337	−1.792	0.050	−0.549	−0.498
	N–H	0.337	−1.800	0.051	−0.549	−0.499
	N–H	0.338	−1.802	0.050	−0.550	−0.500

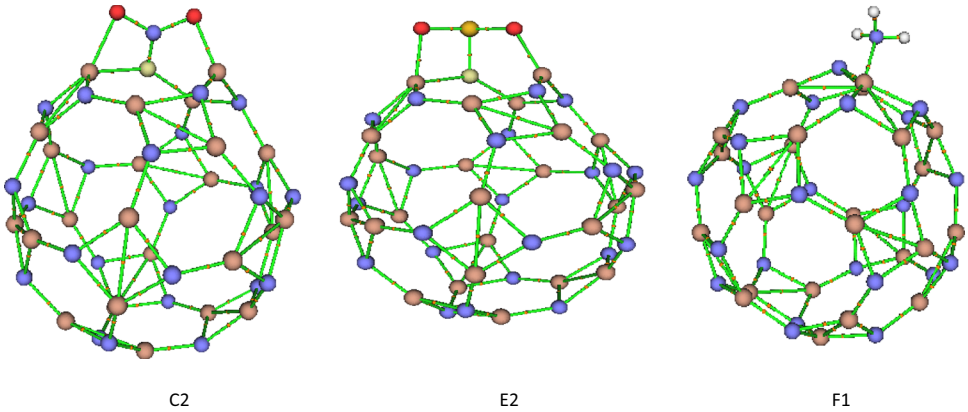

Fig. 12 AIM molecular graphs for C2, E2, and F1

der Waals interactions). Figure 12 displays the BCP between the atoms of the complexes under investigation. As shown in Table 5, the results for the C2 complex indicate that the **N–C** bond should be regarded as a strong polar covalent bond because its ρ_r value is 0.326 a.u, which is somewhat higher than the **S–C** in E2. According to the binding energies, the Al–C ($Al_{24}N_{23}C$) bond in the C2 complex has a higher ρ_r value for BCP than the same bond in the E2 configuration. A weaker association between NH_3 and nanocages is also indicated by the fact that F1′s electron density (0.050 a.u.) is lower than that of C2 and E2. The low values of $\rho_r < 0.1$ for Al–C, Al1–O, Al2–O, and Al–N bonds of SO_2, NO_2, and NH_3 at $Al_{24}N_{24}$ and $Al_{24}N_{23}C$ nanocages show that the charge dissipates in the distance between the two nuclei and that the interactions can be categorized as a closed-shell type, which is related to strong non-covalent interactions [46, 47].

Conclusion

In this paper, the aim was to investigate the use of $Al_{24}N_{24}$ and $Al_{24}N_{23}C$ nanocages toward three harmful gases (NO_2, SO_2, and NH_3). The adsorption properties were determined through adsorption energies, charge transfer, dipole moment, thermodynamic parameters, PDOS, NCI, and QTAIM, and the following results are obtained:

- Introducing carbon-doped increases the adsorption energies for NO_2 and SO_2 gases, while decreasing for NH_3 gas
- The charge is transferred from the NH_3 gas molecule to the nanocage, while for NO_2 and SO_2 systems, the charge transfers from the nanocage to the SO_2 and NO_2 gas molecules except configurations C1 and D1.
- The directions of dipole moment vectors for the NH_3 system point forward to this group, while dipole moment vectors of the SO_2 and NO_2 adsorbed on $Al_{24}N_{24}$ and $Al_{24}N_{23}C$ nanocages point away from these two groups except configuration D1.
- The Gibbs-free energy change (ΔG) for all configurations is negative except that A1 and G2 have a positive value confirming weak adsorption for these complexes.
- The energy gaps decreased after adsorping NO_2, SO_2, and NH_3 on $Al_{24}N_{24}$ and $Al_{24}N_{23}C$ nanocages.
- Higher interaction intensity was observed for C2 and E2 configurations due to the partial covalent contact between the SO_2 and NO_2 molecules with the $Al_{24}N_{23}C$ nanocage.
- The results obtained from QTAIM for the C2 complex indicate that the **N–C** bond should be regarded as a strong polar covalent bond because its ρ_r value is 0.326 a.u and a weaker association between NH_3 and $Al_{24}N_{24}$ nanocages is indicated by electron density (0.050 a.u.) that is lower than that of configuration C2 and E2.

These results confirm that $Al_{24}N_{24}$ and $Al_{24}N_{23}C$ nanocages were used as promising materials for the removal of NO_2, SO_2, and NH_3 toxic gases.

Author contribution Kamal A. Soliman: conceptualization, writing and reviewing the manuscript; A.S.Shalabi: conceptualization and reviewing the manuscript; R. A. Taha: investigation, writing the manuscript; M.M. Assem: reviewing the manuscript.

Funding Open access funding provided by The Science, Technology & Innovation Funding Authority (STDF) in cooperation with The Egyptian Knowledge Bank (EKB).

Data and code availability The authors confirm that the data supporting the findings of this study are available within the article.

Code used for calculated data and analysis is commercial, and the authors have a license to the software.

Declarations

Competing interests The authors declare no competing interests.

Ethical statement We certify that we participated in the design of this work as well as the writing of the manuscript and to assume public responsibility for it. We have reviewed the final version of the manuscript, and we have agreed to publish this manuscript. This manuscript has not been published elsewhere. All the authors are aware and agree to transmission, and no part of the manuscript has previously been published in another journal.

Conflict of interest The authors declare no competing interests.

References

1. Suceska M, Tumara BS, Skrlec V, Stankovic S (2021) Prediction of concentration of toxic gases produced by detonation of commercial explosives by thermochemical equilibrium calculations. Defence Technol 1:2
2. SL Taylor, NA Higley, RK Bush (1986) sulfites in foods: uses, analytical methods, residues, fate, exposure assessment, metabolism, toxicity, and hypersensitivity, in Advances in Food Research, C.O. Chichester, E.M. Mrak, B.S. Schweigert, Editors, Academic Press 1–76
3. Zubieta CE, Fortunato LF, Belelli PG, Ferullo RM (2014) Theoretical study of SO2 adsorption on goethite (110) surface. Appl Surf Sci 314:558–563
4. Ayesh AI (2022) H2S and SO2 adsorption on Cu doped MoSe2: DFT investigation. Phys Lett A 422:127798
5. Liu XY, Zhang JM, Xu KW, Ji V (2014) Improving SO2 gas sensing properties of graphene by introducing dopant and defect: a first-principles study. Appl Surf Sci 313:405–410
6. Ammar HY, Badran HM, Eid KM (2020) TM-doped B12N12 nanocage (TM = Mn, Fe) as a sensor for CO, NO, and NH3 gases: a DFT and TD-DFT study. Mater Today Commun 25:101681
7. Gao C, Zhang Y, Yang H, Liu Y, Liu Y, Du J, Ye H, Zhang G (2019) A DFT study of In doped Tl2O: a superior NO2 gas sensor with selective adsorption and distinct optical response. Appl Surf Sci 494:162–169
8. Beheshtian J, Kamfiroozi M, Bagheri Z, Peyghan AA (2012) B12N12 nano-cage as potential sensor for NO2 detection. Chin J Chem Phys 25(1):60
9. Rad AS, Ateni SG, Tayebi H, Valipour P, Foukolaei VP (2016) First-principles DFT study of SO2 and SO3 adsorption on 2PANI: a model for polyaniline response. J Sulfur Chem 37(6):622–631
10. Tian Y, Qu K, Zeng X (2017) Investigation into the ring-substituted polyanilines and their application for the detection and adsorption of sulfur dioxide. Sensors Actuators B: Chem 249:423–430
11. Liu H, Wang F, Hu K, Li T, Yan Y, Li J (2021) The adsorption and sensing performances of Ir-modified MoS2 monolayer toward SF6 decomposition products: a DFT study. Nanomaterials 11(1):100
12. Beheshtian J, Soleymanabadi H, Peyghan AA, Bagherid Z (2013) A DFT study on the functionalization of a BN nanosheet with PCX,(PC= phenyl carbamate, X= OCH3, CH3, NH2, NO2 and CN). Appl Surf Sci 268:436–441
13. Chang H, Lee JD (2001) Adsorption of NH3 and NO2 molecules on carbon nanotubes. Appl Phys Lett 79(23):3863–3865
14. Beheshtian J, Peyghan AA, Bagheri Z (2013) Functionalization of BN nanosheet with N 2 H 4 may be feasible in the presence of Stone-Wales defect. Struct Chem 24(5):1565–1570
15. Wang C, Luo X, Zhang S, Shen Q, Zhang L (2014) Effects of nitrogen gas ratio on magnetron sputtering deposited boron nitride films. Vacuum 103:68–71
16. Beheshtian J, Peyghan AA, Bagheri Z, Kamfiroozi M (2012) Interaction of small molecules (NO, H 2, N 2, and CH 4) with BN nanocluster surface. Struct Chem 23(5):1567–1572
17. Bagheri Z, Peyghan AA (2013) DFT study of NO2 adsorption on the AlN nanocones. Comput Theor Chem 1008:20–26
18. Beheshtian J, Peyghan AA, Tabar MB, Bagheri Z (2013) DFT study on the functionalization of a BN nanotube with sulfamide. Appl Surf Sci 266:182–187
19. Beheshtian J, Peyghan AA, Bagheri Z (2013) Sensing behavior of Al-rich AlN nanotube toward hydrogen cyanide. J Mol Model 19(6):2197–2203
20. Yum K, Yu MF (2006) Measurement of wetting properties of individual boron nitride nanotubes with the Wilhelmy method using a nanotube-based force sensor. Nano Lett 6(2):329–333
21. Mekawy M, Salih RYE, Hassan A, El-Sherbiny IM (2016) Synthesis, characterization and electrochemical-sensor applications of zinc oxide/graphene oxide nanocomposite. J Nanostruct Chem 6(2):137–144
22. Soltani A, Peyghan AA, Bagheri Z (2013) H2O2 adsorption on the BN and SiC nanotubes: A DFT study. Physica E 48:176–180
23. Zhi C, Bando Y, Tang C, Golberg D (2010) Boron nitride nanotubes. Mater Sci Eng R Rep 70(3):92–111
24. Kostoglou N, Polychronopoulou K, Rebholz C (2015) Thermal and chemical stability of hexagonal boron nitride (h-BN) nanoplatelets. Vacuum 112:42–45
25. Sameti MR, Jamil ES (2016) The adsorption of CO molecule on pristine, As, B, BAs doped (4, 4) armchair AlNNTs: a computational study. J Nanostruct Chem 6(3):197–205
26. Fadlallah MM, Maarouf AA, Soliman KA (2019) Boron nitride nanocones template for adsorbing NO2 and SO2: an ab initio investigation. Physica E 113:188–193
27. Zhang Z, Liang B, Chi Y, Jiang Y, Song J, Guo Y (2021) Adsorption mechanism of SO2 on vacancy-defected graphene and Ti doped graphene: a DFT study. Superlattices Microstruct 159:107036
28. Halim WS, Assem MM, Shalabi AS, Soliman KA (2009) CO adsorption on Ni, Pd, Cu and Ag deposited on MgO, CaO, SrO and BaO: density functional calculations. Appl Surf Sci 255(17):7547–7555
29. Derdare M, Boudjahem AG, Boulbazine M (2021) Adsorption of the NO2, N2O and NH3 molecules over the C20 and MC19 (M = Ru, Ir and Au) clusters: a DFT approach. Surfaces Interfaces 24:101114
30. Zahedi E, Seif A (2011) Adsorption of NH3 and NO2 molecules on C48B6N6 heterofullerene: a DFT study on electronic properties. Physica B 406(19):3704–3709
31. Rad AS, Esfahanian M, Maleki S, Gharati G (2016) Application of carbon nanostructures toward SO2 and SO3 adsorption: a comparison between pristine graphene and N-doped graphene by DFT calculations. J Sulfur Chem 37(2):176–188
32. Basharnavaz H, Habibi-Yangjeh A, Kamali SH (2020) Adsorption performance of SO2 gases over the transition metal/P-codoped graphitic carbon nitride: a DFT investigation. Mater Chem Phys 243:122602
33. Noei M (2017) Different electronic sensitivity of BN and AlN nanoclusters to SO2 gas: DFT studies. Vacuum 135:44–49
34. Rad AS, Ayub K (2017) O3 and SO2 sensing concept on extended surface of B12N12 nanocages modified by nickel decoration: a comprehensive DFT study. Solid State Sci 69:22–30
35. Xi M, He C, Yang H, Fu X, Fu L, Cheng X, Guo J (2022) Predicted a honeycomb metallic BiC and a direct semiconducting Bi2C monolayer as excellent CO2 adsorbents. Chin Chem Lett 33:2595–2599

36. Zhao C, Xi M, Huo J, He C, Fu L (2023) Computational design of BC3N2 based single atom catalyst for dramatic activation of inert CO2 and CH4 gasses into CH3COOH with ultralow CH4 dissociation barrier. Chin Chem Lett 34:107213
37. Huo J, Wei H, Fu L, Zhao C, He C (2023) Highly active Fe36Co44 bimetallic nanoclusters catalysts for hydrolysis of ammonia borane: The first-principles study. Chin Chem Lett 34:107261
38. Zhang L, Yang X, Zhang L, Shu H, Jia Y, Qi L, Han Y, Wang R (2022) Preparation of nano-hollow sphere hydrolytic catalyst and study on its COS removal performance. J Nanoparticle Res 24:268
39. Zhao C, Xi M, Huo J, He C (2021) B-Doped 2D-InSe as a bifunctional catalyst for CO2/CH4 separation under the regulation of an external electric field. Phys Chem Chem Phys 23:23219–23224
40. Gaussian 09, Revision C.01, Frisch MJ, Trucks GW, Schlegel HB, Scuseria GE, Robb MA, Cheeseman JR, Scalmani G, Barone V, Mennucci B, Petersson GA, Nakatsuji H, Caricato M, Li X, Hratchian HP, Izmaylov AF, Bloino J, Zheng G, Sonnenberg JL, Hada M, Ehara M, Toyota K, Fukuda R, Hasegawa J, Ishida M, Nakajima T, Honda Y, Kitao O, Nakai H, Vreven T, Montgomery JA Jr, Peralta JE, Ogliaro F, Bearpark M, Heyd JJ, Brothers E, Kudin KN, Staroverov VN, Kobayashi R, Normand J, Raghavachari K, Rendell A, Burant JC, Iyengar SS, Tomasi J, Cossi M, Rega N, Millam NJ, Klene M, Knox JE, Cross JB, Bakken V, Adamo C, Jaramillo J, Gomperts R, Stratmann RE, Yazyev O, Austin AJ, Cammi R, Pomelli C, Ochterski JW, Martin RL, Morokuma K, Zakrzewski VG, Voth GA, Salvador P, Dannenberg JJ, Dapprich S, Daniels AD, Farkas Ö, Foresman JB, Ortiz JV, Cioslowski J, Fox DJ (2009) Gaussian Inc., Wallingford CT
41. Hong VM, Ng H, Huang K, Zhou PS, Lee W, Que JZX, Kong LB (2017) Recent progress in layered transition metal carbides and/or nitride (MXenes) and their composites: synthesis and applications. J Mater Chem A 5:3039–3068
42. Khakbaz P, Moshayedi M, Hajian S, Soleimani M, Narakathu BB, Bazuin BJ, Pourfath M, Atashbar MZ (2019) Titanium carbide MXene as NH sensor: realistic first-principles study. J Phys Chem C 123(49):29794–29803
43. Khazaei M, Ranjbar A, Arai M, Sasaki T, Yunoki S (2017) Electronic properties and applications of MXenes: a theoretical review. J Mater Chem C 5:2488–2503
44. Matta CF (2006) Hydrogen–hydrogen bonding: the non-electrostatic limit of closed-shell interaction between two hydro, hydrogen bonding-new insights 3:337–375
45. Zhang L, Qi ZD, Ye YL, Li XH, Chen JH, Sun W-M (2021) DFT study on the adsorption of 5-fluorouracil on B40, B39M, and M@B40 (M = Mg, Al, Si, Mn, Cu, Zn), RSC Advances, 11 39508–39517
46. Asif M, Sajid H, Ayub K, Ans M, Mahmood T (2022) A first principles study on electrochemical sensing of highly toxic pesticides by using porous C4N nanoflake. J Phys Chem Solids 160:110345
47. Shakerzadeh E, Kazemimoghadam F (2021) Magnesiation of bare and halides encapsulated B40 fullerenes for their potential application as promising anode materials for Mg-ion batteries. Appl Surf Sci 538:148060